

## Structure of *Escherichia coli* Aminodeoxychorismate Synthase: Architectural Conservation and Diversity in Chorismate-Utilizing Enzymes<sup>†,‡</sup>

James F. Parsons,<sup>§</sup> Pia Y. Jensen,<sup>§</sup> Abraham S. Pachikara,<sup>§</sup> Andrew J. Howard,<sup>||</sup> Edward Eisenstein,<sup>\*,§,⊥</sup> and Jane E. Ladner<sup>\*,§</sup>

Center for Advanced Research in Biotechnology, University of Maryland Biotechnology Institute, National Institute of Standards and Technology, 9600 Gudelsky Drive, Rockville, Maryland 20850, Department of Chemistry and Biochemistry, University of Maryland Baltimore County, Baltimore, Maryland 21228, and Biological, Chemical, and Physical Sciences Department, Illinois Institute of Technology, Chicago, Illinois 60616

Received September 21, 2001; Revised Manuscript Received November 21, 2001

**ABSTRACT:** Aminodeoxychorismate synthase is part of a heterodimeric complex that catalyzes the two-step biosynthesis of 4-amino-4-deoxychorismate, a precursor of *p*-aminobenzoate and folate in microorganisms. In the first step, a glutamine amidotransferase encoded by the *pabA* gene generates ammonia as a substrate that, along with chorismate, is used in the second step, catalyzed by aminodeoxychorismate synthase, the product of the *pabB* gene. Here we report the X-ray crystal structure of *Escherichia coli* PabB determined in two different crystal forms, each at 2.0 Å resolution. The 453-residue monomeric PabB has a complex  $\alpha/\beta$  fold which is similar to that seen in the structures of homologous, oligomeric TrpE subunits of several anthranilate synthases of microbial origin. A comparison of the structures of these two classes of chorismate-utilizing enzymes provides a rationale for the differences in quaternary structures seen for these enzymes, and indicates that the weak or transient association of PabB with PabA during catalysis stems at least partly from a limited interface for protein interactions. Additional analyses of the structures enabled the tentative identification of the active site of PabB, which contains a number of residues implicated from previous biochemical and genetic studies to be essential for activity. Differences in the structures determined from phosphate- and formate-grown crystals, and the location of an adventitious formate ion, suggest that conformational changes in loop regions adjacent to the active site may be needed for catalysis. A surprising finding in the structure of PabB was the presence of a tryptophan molecule deeply embedded in a binding pocket that is analogous to the regulatory site in the TrpE subunits of the anthranilate synthases. The strongly bound ligand, which cannot be dissociated without denaturation of PabB, may play a structural role in the enzyme since there is no effect of tryptophan on the enzymic synthesis of aminodeoxychorismate. Extensive sequence similarity in the tryptophan-binding pocket among several other chorismate-utilizing enzymes, including isochorismate synthase, suggests that they too may bind tryptophan for structural integrity, and corroborates early ideas on the evolution of this interesting enzyme family.

The biosynthesis of *p*-aminobenzoic acid (PABA)<sup>1</sup> from chorismate in plants and microorganisms occurs via two reactions (1). First, chorismate and ammonia, derived from glutamine, are converted to 4-amino-4-deoxychorismate

(ADC) and glutamate via the action of an interesting, heterodimeric complex of the *pabA* and *pabB* gene products (2–5). In the second reaction, a pyridoxal phosphate-dependent ADC lyase encoded by the *pabC* gene converts ADC to PABA, a precursor to folic acid (Scheme 1) (1, 6, 7). In *Escherichia coli*, the 51 kDa PabB protein (ADC synthase; component I of PABA synthase) binds chorismate and utilizes ammonia to catalyze the formation of ADC. Physiologically, ammonia is supplied via glutamine hydrolysis by the 21 kDa PabA component of the enzyme, which appears to belong to the class I (G-type) glutamine amidotransferases (1, 6–8). However, the PabB component can function in solution without PabA if ammonia is supplied (1, 9). Although PabA and PabB have not been isolated as a stable oligomeric complex, and there are conflicting reports regarding the extent of association between PabA and PabB (10, 11), it is certain that the enzymes associate at least transiently for glutamine-dependent ADC production.

<sup>†</sup> This work was supported in part by NSF Grant MCB 23086 (to E.E.).

<sup>‡</sup> Coordinates for PabB in the formate and phosphate crystal forms have been deposited in the RCSB Protein Data Bank as entries 1K0E and 1K0G, respectively.

\* To whom correspondence should be addressed: Center for Advanced Research in Biotechnology, 9600 Gudelsky Dr., Rockville, MD 20850. E-mail: jane.ladner@nist.gov and edd@carb.nist.gov.

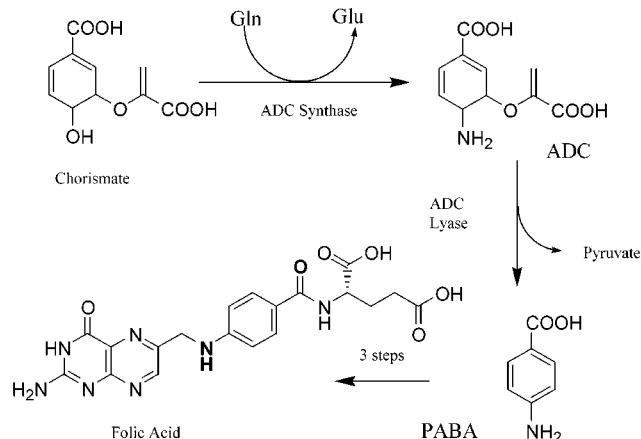
<sup>§</sup> Center for Advanced Research in Biotechnology.

<sup>||</sup> Illinois Institute of Technology.

<sup>⊥</sup> University of Maryland Baltimore County.

<sup>1</sup> Abbreviations: PABA, *p*-aminobenzoic acid; ADC, 4-amino-4-deoxychorismate; MAD, multiwavelength anomalous dispersion; TrpE-ss, TrpE subunit of anthranilate synthase from *S. solfataricus* (AS-ss) (PDB entry 1QDL); TrpE-st, TrpE subunit of anthranilate synthase from *Sa. typhimurium* (AS-st) (PDB entry 1H1Q); TrpE-sm, TrpE subunit of anthranilate synthase from *Se. marcescens* (AS-sm) (PDB entries 1I7S and 1I7Q); ADIC, aminodeoxyisochorismate.

Scheme 1: Enzymic Production of PABA, a Precursor to Folic Acid in Microorganisms



Although ADC synthase displays some striking similarities to other chorismate-utilizing enzymes in aromatic compound biosynthesis in plants and microorganisms (8, 9, 12, 13), there are several unexplained differences in the enzymes catalyzing the biosynthesis of PABA relative to those involved in other chorismate transmutations. One of the enzymes most similar to ADC synthase is anthranilate synthase, which provides a branch for chorismate utilization in the biosynthesis of tryptophan. Anthranilate synthases are invariably stable oligomeric proteins, consisting of at least two different subunits encoded by the *trpE* and *trpG* genes, the sequences of which are highly similar to those of the *pabB* and *pabA* genes, respectively (12, 14–17). The TrpE subunit of anthranilate synthase is a bifunctional enzyme that first converts chorismate and ammonia to 2-amino-2-deoxyisochorismate and then converts this product to anthranilate via the elimination of pyruvate (18, 19). Thus, the biosynthesis of anthranilate does not require another enzyme for pyruvate elimination from an aminated chorismate intermediate as seen in the PABA pathway. The TrpG subunit of anthranilate synthases functions as a glutamine amidotransferase to provide ammonia for addition to chorismate by TrpE (8, 20).

Unlike PabB and PabA, the TrpE and TrpG subunits are tightly associated in stable dimeric or tetrameric complexes with 1:1 or 2:2 TrpE:TrpG stoichiometry, and are generally not found as monomers (17). High-resolution structures for tetrameric anthranilate synthases from *Sulfolobus solfataricus* (21), *Salmonella typhimurium* (22), and *Serratia marcescens* (23) have recently been described. Although the overall folds of the enzymes are significantly similar, their quaternary structures are surprisingly unique, and may relate to their pattern of regulation by tryptophan, the end product of the pathway (22). No similar control mechanism has been detected for the enzymes involved in PABA biosynthesis (5).

This work describes the 2.0 Å resolution crystal structure of PabB, ADC synthase, determined in two crystal forms. The overall fold of PabB is similar to that seen for oligomeric anthranilate synthases. However, several striking differences in these structures provide an explanation for the monomeric nature of ADC synthase, and suggest why it is unable to catalyze the two-step conversion of chorismate to PABA itself. A surprising discovery revealed by the structure is that

tryptophan is bound to a site analogous to the regulatory sites in the anthranilate synthases. Because this ligand has no effect on the catalytic properties of ADC synthase and, indeed, is unable to be removed except by denaturation of the enzyme, it is suggested to play a structural role in ADC synthase. The high degree of sequence similarity between several other chorismate-utilizing proteins with ADC synthase and anthranilate synthase suggests that the isochorismate synthases encoded by the *menF* and *entC* genes may also bind tryptophan in a structural capacity, and sheds interesting light on the evolutionary relationships among this family of enzymes.

## MATERIALS AND METHODS

**Enzyme Expression and Purification.** *E. coli* PabB was expressed in *E. coli* BL21 cells using the expression plasmid pKPabB, a derivative of pKK233-2 (Pharmacia) that contains the *pabB* gene under the control of the *trc* promoter. Cells were grown in shaker flasks at 37 °C to a density of 1.0 at 600 nm, and protein production was induced by the addition of IPTG to a final concentration of 1 mM. Shaking was continued for an additional 4 h, at which time cells were harvested by centrifugation. Purification was achieved using a modification of the method of Nichols (5). Briefly, cells were suspended in 10 mM Tris-HCl, 1 mM EDTA, and 1 mM DTT (pH 8.0) and lysed by sonication. Insoluble cell debris was removed by centrifugation at 35000g. The soluble material was filtered and applied to a Poros HQ50 column (10 cm × 40 cm) (PerSeptive) previously equilibrated with the above buffer and attached to a BioCad 700E purification workstation. The bound material, including PabB, was eluted with a 0 to 1.0 M gradient of NaCl in the same buffer. The PabB-containing fractions were pooled, concentrated, and dialyzed against 10 mM KH<sub>2</sub>PO<sub>4</sub>, 0.1 mM EDTA, and 1 mM DTT (pH 6.7). The dialysate was then applied to a Poros HS20 cation exchange column (PerSeptive) (5 cm × 20 cm) and a hydroxyapatite column (Bio-Rad) (5 cm × 20 cm) attached in tandem to the BioCad instrument. PabB was collected from the flow through while significant contaminants remained bound. The PabB-containing material was then concentrated and dialyzed against 10 mM MOPS, 0.1 mM EDTA, and 1 mM DTT (pH 7.6) before being applied to a 5 cm × 50 cm Poros HQ20 (PerSeptive) column equilibrated with the same buffer. PabB was eluted with a 0 to 0.25 M gradient of NaCl. Fractions judged to be pure by gel electrophoresis in the presence of SDS were pooled, dialyzed against 50 mM MOPS, 50 mM KCl, 0.1 mM EDTA, 2 mM DTT, and 5 mM MgCl<sub>2</sub> (pH 7.6), concentrated to 15–20 mg/mL, and stored at –80 °C. The yield was commonly 50–60 mg of pure PabB per liter of culture.

The formation of aminodeoxychorismate catalyzed by PabB was assayed in a coupled reaction with an excess of purified PabC enzyme by monitoring the formation of *p*-aminobenzoic acid at 272 nm ( $\Delta\epsilon = 17\,000\text{ M}^{-1}\text{ cm}^{-1}$ ) in buffer containing 50 mM HEPES, 10 mM MgCl<sub>2</sub>, 1 mM DTT, 0.1 M (NH<sub>4</sub>)<sub>2</sub>SO<sub>4</sub>, and 30 μM chorismic acid. The specific activity of PabB under these conditions and at 25 °C was 0.07 s<sup>-1</sup>.

The selenomethionine-labeled protein was expressed as previously described (24), and purified in the same manner as the native protein. The yield was approximately 40 mg per liter of culture.

Table 1: Se MAD Data and Phasing Statistics

	low remote	edge	peak
wavelength (Å)	0.9686	0.9793	0.9790
resolution (Å)	41.0–2.22	41.0–2.22	41.0–2.22
no. of observations	332187	326780	318226
no. of reflections	88614	86012	86097
completeness (%)	97	94	94
$R_{\text{sym}}$	0.062	0.062	0.059
phasing			
acentric phasing power	16.7	23.4	14.4
iso/aniso phasing power	3.6	3.3	2.7
$R_{\text{Cullis}}$ , acentric	0.11	0.06	0.11
$R_{\text{Cullis}}$ , iso/aniso	0.53	0.57	0.69
figure of merit before flattening	0.44		
figure of merit after flattening	0.84 (with extension)		

**Crystallization.** Crystallization conditions were surveyed by the hanging drop vapor diffusion method at room temperature using Crystal Screen Kit I from Hampton Research (Laguna Niguel, CA). The protein solution contained 50 mM MOPS (pH 7.4), 50 mM KCl, 5 mM MgCl<sub>2</sub>, 2 mM DTT, and 40.2 mg/mL protein. The hanging drops were made from equal volumes of protein solution and well solution. For the formate crystals, the wells contained 0.1 M sodium acetate (pH 4.6) and 2.0 M sodium formate, and the crystals grew to dimensions of 0.3 mm × 0.3 mm × 0.3 mm in ~7 days. For the phosphate crystals, the wells contained 0.1 M sodium HEPES (pH 7.5), 0.8 M sodium phosphate, and 0.8 M potassium phosphate, and the crystals grew to dimensions of 0.2 mm × 0.2 mm × 0.1 mm in ~2 days. The selenomethionine protein crystals were grown under the same sodium formate conditions, but the protein concentration was 26.2 mg/mL.

**Synchrotron Data Collection.** Diffraction data for the formate crystals and the selenomethionine crystals were collected at IMCA-CAT beamline 17BM-B at the Advanced Photon Source of Argonne National Laboratory (Argonne, IL) using a MarCCD and a Mar345 (Mar Research) detector at 200 and 170 mm, respectively. The wavelength for the formate crystal was 1.0 Å; the selenomethionine data were collected at 0.9790, 0.9793, and 0.9686 Å. The crystals were cryoprotected by dipping them in a solution that was 50% well solution and 50% saturated lithium formate (25). Diffraction data for the phosphate crystal were collected at IMCA-CAT beamline 17ID-B using a MarCCD (Mar Research) detector at 140 mm. The wavelength was 1.06 Å, and the crystal was cryoprotected by dipping it in a solution that was 30% glycerol and 70% well solution. The temperature of the crystals during data collection was maintained near 115 K using a cooled nitrogen stream from an Oxford cryostream (Oxford Cryosystems).

The diffraction data for the selenomethionine and phosphate crystals were processed using X-GEN (26). The diffraction data for the formate crystals were processed using d\*TREK (27). Statistics on the MAD data are shown in Table 1.

**Structure Determinations.** The structure of PabB was determined using the MAD data from a selenomethionine formate crystal. PabB has eight methionines in each polypeptide chain, and there are two polypeptide chains in the asymmetric unit. The program SHELXD (28) was used to find a cluster of 14 selenium positions (N-terminal methionines are frequently disordered). SHARP (29) was used for heavy atom phasing and refinement and for solvent flattening

(30). The initial map was uninterpretable, but when the cluster of atoms was inverted, the map was quite good. The program ARP/wARP (31) was used to build the initial model. The structure of PabB in the phosphate crystal form was determined by molecular replacement using the structure for the formate crystals as a model with the program suite CNS (32). ARP/wARP (31) was used to rebuild the model following the initial placement to remove model bias.

XtalView was used to view the models graphically, to construct portions not built by ARP/wARP, and to adjust the models during refinement (33). SHELX (34) was used to refine the models against their respective diffraction data. Turbo-Frodo (35) was used to align and view structures from different crystal forms and different biological sources. The Protein Data Bank (36) was searched for molecules with structural homology using CE (37). The stereochemistry of the models was checked with PROCHECK (38). The secondary structure was analyzed with DSSP (39) and PROMOTIF (40). WATERTIDY and SORTWATER from the CCP4 (41) package were used to examine the water structure. The data and refinement statistics are shown in Table 2.

## RESULTS

**Overall Structure.** As can be seen in Figure 1, the 453-residue PabB enzyme has a complex  $\alpha/\beta$  fold similar to that seen in the anthranilate synthase structures from *S. solfataricus* (AS-ss) (PDB entry 1QDL), *Sa. typhimurium* (AS-st) (PDB entry 1I1Q) and *Se. marcescens* (AS-sm) (PDB entries 1I7S and 1I7Q) (21–23). The core of the enzyme is composed of two domains that form a  $\beta$ -sheet sandwich with helices and loops on the outside. A structural alignment of PabB with the anthranilate synthase structures using CE (37) indicates a high degree of structural similarity, with the results presented in Table 3. Inspection of the topology diagram shown in Figure 2 reveals that there are two areas of the structure that are similar in PabB, AS-st and AS-sm, but which are absent in the *Sulfolobus* enzyme. There is a  $\beta$ -hairpin between residues 60 and 78 in PabB, which extends the  $\beta$ -sheet of the so-called second domain, and an  $\alpha$ -helix at residues 159–170 that bridges the two halves of the first domain. In the formate-grown crystals, no density was seen for residues 1, 2, and 280–292 in molecule A and for residues 272–296 and 328–341 in molecule B; crystals grown in phosphate did not exhibit density for residues 275–298 and 331–339 in molecule A and residues 276–300 and 329–339 in molecule B. The rms deviation for the C $\alpha$  atoms between the two chains in the formate crystals is 0.6 Å for 388 of a possible 414 common residues and 0.4 Å for the two chains in the phosphate crystals for 389 of a possible 415 common residues. The rms deviation for the comparison of chain A from each crystal form is 0.5 Å for 420 common residues. The residues that were excluded in these comparisons include those around the active site and in the loop from residues 39 to 42 above the tryptophan-binding site. A structure-based sequence alignment of PabB with the TrpE subunits of anthranilate synthases from *Se. marcescens* (1I1Q) and *S. solfataricus* (1QDL) is presented in Figure 3.

**Comparison of PabB Structures from Different Crystal Forms.** A comparison of the structures from crystals grown in formate and those in phosphate is rather interesting. The

Table 2: Data Collection and Refinement Statistics

	phosphate crystals	formate crystals
diffraction data		
space group	$P2_12_12_1$	$P2_12_12$
cell parameters ( $a, b, c$ ) (Å)	102.01, 109.71, 134.38	111.99, 185.72, 45.01
content of asymmetric unit	two chains	two chains
$V_m$ (Å <sup>3</sup> /Da) (% solvent content)	3.7 (67)	2.3 (47)
wavelength of data collection (Å)	1.0597	1.000
no. of measured intensities	348268	269253
no. of unique reflections	88221	55584
resolution of data (Å)	2.05	2.00
highest-resolution shell (Å)	2.16–2.05	2.08–2.00
$R_{\text{sym}}$ (overall/high-resolution shell)	0.063/0.327	0.100/0.208
completeness (%) (overall/high-resolution shell)	99.6/98.6	91.2/90.4
redundancy (overall/high-resolution shell)	4/4	5/3
mean $I/\sigma$ (overall/high-resolution shell)	28.1/2.7	11.5/4.8
refinement		
refinement program	SHELX	SHELX
resolution limits (Å)	10.0–2.05	10.0–2.00
$R$ -factor (95% of data)	0.173	0.205
$R_{\text{free}}$ (5% of data)	0.238	0.315
residues included (chain A/chain B)	420/416	438/414
hetero groups (not water molecules)	two phosphate ions, two tryptophans	one formate ion, two tryptophans
no. of water molecules	548	313
bond length rms deviation (Å)	0.021	0.021
angle distance rms deviation (Å)	0.057	0.061
plane rms deviation (Å)	0.023	0.018
% in allowed and most favored regions of Ramachandran plot	98.9	98.3
average $B$ (main chain/side chain)	25.5/33.1	26.2/32.6
average water molecule $B$	39.4	30.1

phosphate crystals have a very high solvent content (67%), but are quite rigid; the data are strong to 2 Å, and the structure refines well. As can be seen in Figure 4A, these characteristics may possibly be attributable to the strong interactions between the two polypeptides that are found in the asymmetric unit as evidenced by the 1898 Å<sup>2</sup> of surface area that is buried between them. In addition, there are extensive interactions between neighboring molecules in different asymmetric units. Interestingly, the interactions between adjacent, symmetry-related monomers may be relatively strong since they disrupt the native helical conformation of residues 303–309 seen in the formate-grown crystals, and result in a significant dislocation of this segment away from the local environment of the active site. This unfolded region in PabB is close to the area that, by comparison to the structures of anthranilate synthase, would contribute to the interface for association with the companion glutamine amidotransferase protein, PabA. Although these interactions and unusual conformation are doubtless unrelated to the biological function of PabB, they demonstrate the potential for flexibility in this portion of the molecule.

In contrast, the structures of PabB determined using the crystals obtained from formate do not display significant contact with symmetry-related molecules. Whereas phosphate is present in both molecules in the asymmetric unit, formate is bound in a different location (presumably the active site), and is only present in a single monomer. Interestingly, as can be seen in Figure 4B, the binding of formate leads to pronounced conformational changes in one of the molecules in the asymmetric unit that comprises a portion of the active site. This overlay of the crystal forms containing phosphate (yellow) and formate (color scheme as described in the legend of Figure 1) shows that in the formate-bound monomer, as well as in the second molecule in the asymmetric unit (which is not shown), residues 301–315 adopt

their native, helical structure analogous to that seen in the various structures for TrpE. Thus, the alternative crystal packing stabilized by formate binding permits a glimpse of a portion of the active site that was obscured in phosphate-grown crystals. Another important difference between the crystal forms is that whereas residues 331–339 are disordered in both monomers of the crystals grown in phosphate, as well as in the unliganded monomer of the formate-grown crystals, this region forms a pair of  $\beta$ -strands in the formate-bound monomer that becomes an ordered “flap” (pink). Moreover, the structural differences seen in the formate-liganded flap region relative to the other structural forms may reflect a conformational change promoted by active site ligands that could be important for catalysis (see below).

The crystals grown in formate displayed a relatively high  $R$ -factor, and  $R_{\text{free}}$ , as well as a significant difference between  $R$  and  $R_{\text{free}}$ , which probably stems from the weak diffraction data from this loosely packed crystal form (see Table 2). On the other hand, the strong interactions seen between monomers in the crystals grown from phosphate, even with their unusually high solvent content, led to a well-refined structure. Finally, although two molecules of PabB were present in the asymmetric unit of both crystal forms, the interface is different in each case, consistent with the monomeric structure of PabB seen in solution.

*Probable Active Site Environment.* Although the location of the formate ion in one of the crystal forms and an analysis by Nichols and co-workers on the role of conserved amino acids and inactive mutational variants (11) provided some clues about the probable location of the active site of ADC synthase, the most useful information was gleaned from a comparison of the structure of PabB with the structure of anthranilate synthase from *Se. marcescens* determined with Mg<sup>2+</sup>, benzoic acid, and pyruvate in the TrpE subunit and a  $\gamma$ -glutamyl thioester in the TrpG subunit (23). In the inhibited



FIGURE 1: Ribbon diagram of the structure of PabB from crystals grown in formate solutions. The two major domains of PabB are shown in white and green, and the flap that covers the putative active site in one molecule of the PabB–formate crystal form is shown in pink. Segments of the structure shown in cyan represent elements that are deleted in the sequence and structure of TrpE from *S. solfataricus* but are present, or even extended, in PabB and the TrpE chains from *Sa. typhimurium* and *Se. marcescens*. Space filling models in the CPK color scheme are used to illustrate the positions of the bound tryptophan and a formate ion.

Table 3: Comparison of PabB Formate Chain A with TrpE Structures

	rmsd of C $\alpha$ atoms (Å)	% identity of sequence	no. of residues aligned
TrpE-ss	2.4	30.4	404
TrpE-st	2.5	28.2	428
TrpE-sm with substrates	2.1	30.1	402
TrpE-sm with Trp	2.5	28.7	429

TrpE structure, residues 387–401 constitute a dynamic flap that is displaced by as much as 8 Å from the unliganded enzyme. This flap is homologous to residues 328–342 in PabB, which are disordered in one monomer of the formate crystal form, and in both monomers of the phosphate crystals. However, in one of the monomers of the formate crystals, the flap is structured (shown in pink in Figure 4B), and electron density near R410 fits a formate ion, which corresponds to the region where pyruvate is seen in TrpE of AS-sm. This suggests that in both enzymes, the binding of substrates and inhibitors results in a conformational change in the flap residues that closes the active site. The structural similarities of PabB and TrpE have enabled tentative identification of key residues in the active site.

As can be seen in Figure 5, there are several highly conserved aspects of the active site between PabB and other chorismate-utilizing enzymes. Several invariant residues can

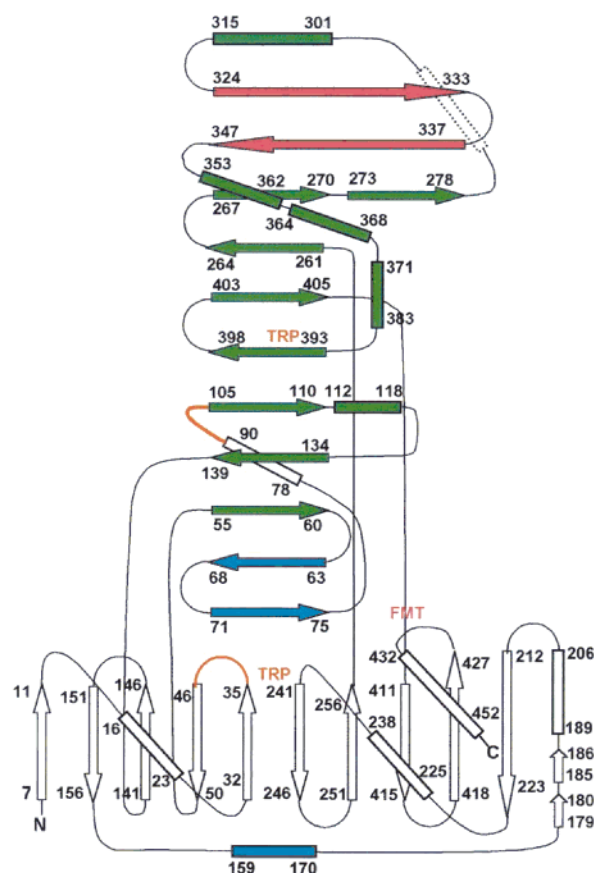


FIGURE 2: Secondary structure and general organization of PabB.  $\beta$ -Strands, shown as arrows, and helices, represented by rectangles, are numbered to indicate the residues that comprise regular secondary structural components. Orange segments and the label TRP identify spatially proximal structural elements in the tryptophan-binding site; the orange loops appear to be encasing or burying the binding site. The pink label FMT indicates the structural elements adjacent to the formate ion that is bound to Arg410; this region corresponds to the active site by comparison with the anthranilate synthases. The structural elements shown in cyan are deleted in the sequence and structure of TrpE from *S. solfataricus*. The helix shown in dotted lines is disordered in PabB, but is predicted by homology to TrpE. The colors of the strands and helices are as described in the legend of Figure 1.

be implicated in the coordination of  $Mg^{2+}$ , which is required for the biosynthesis of ADC and anthranilate, including E302, E439, and the carboxylate of the substrate and/or product, which make direct contacts with the metal, and D299 and E436, which use water to mediate their interaction. Interestingly, in PabB there is a water molecule within approximately 1 Å of the superimposed  $Mg^{2+}$  site. There is also a high level of conservation among the constellation of residues between TrpE and PabB that surround the putative substrate-binding site. It is perhaps surprising that the enzymes display such significant similarity in the pyruvate/formate binding region, especially since the pyruvoyl moiety is cleaved to yield anthranilate in TrpE, whereas ADC is released from PabB. One interesting difference between the two active sites is the presence of K274 in PabB; the corresponding residue in anthranilate synthases and in other chorismate-utilizing enzymes is alanine. The  $\epsilon$ -amino group of K274 site is within

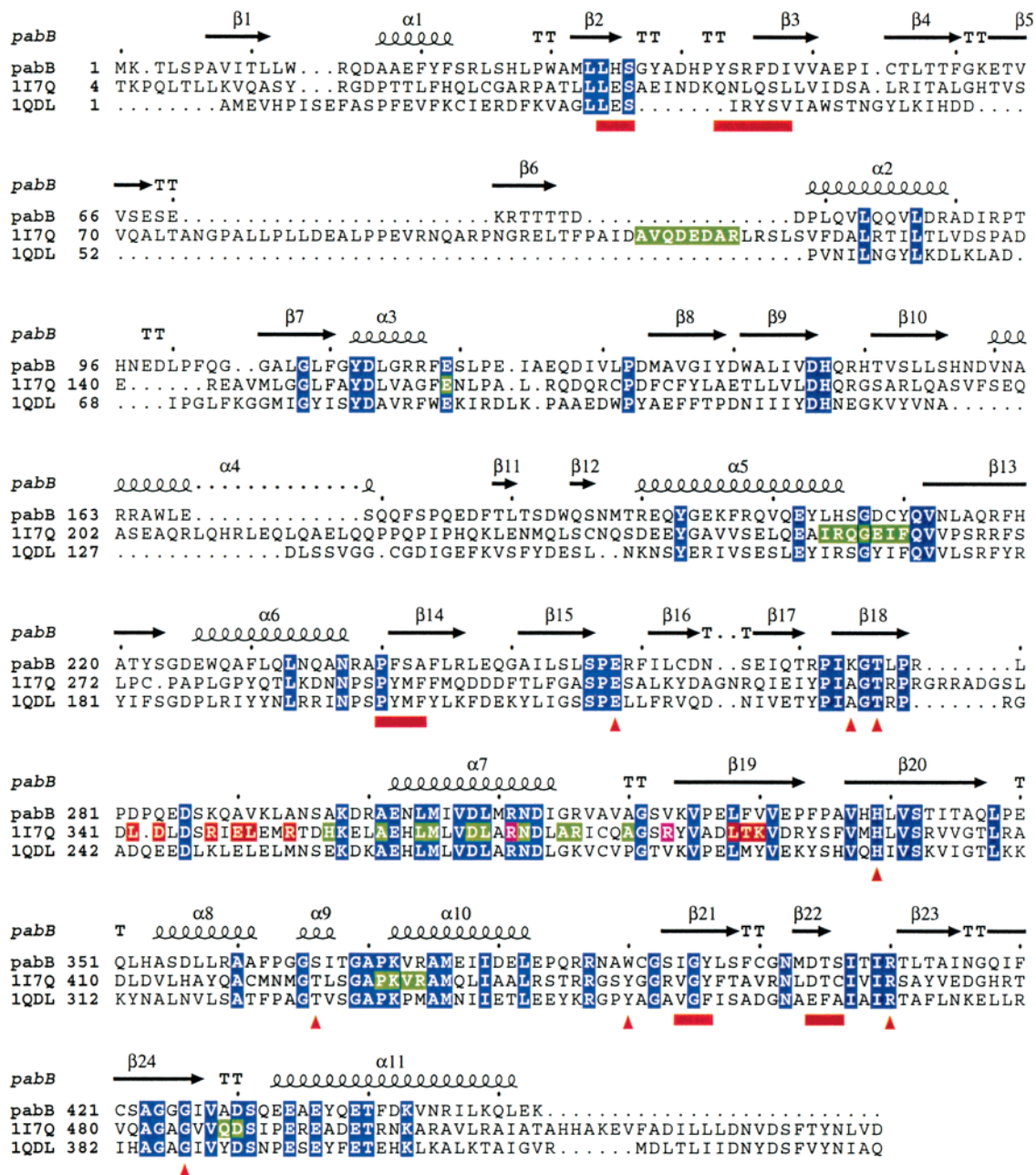


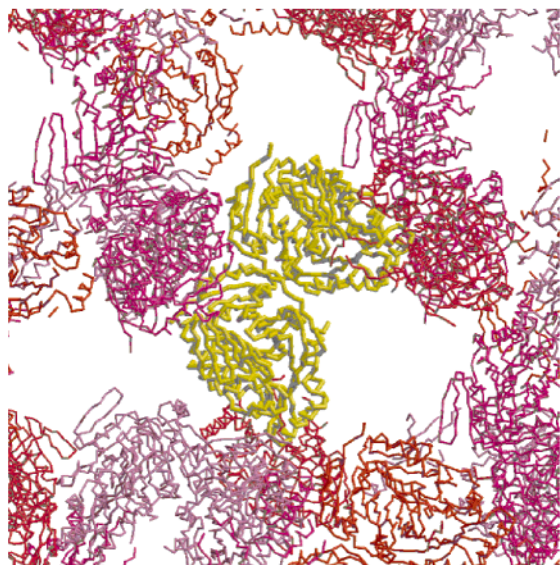
FIGURE 3: Structure-based sequence alignment of *E. coli* PabB, and TrpE from *Se. marcescens* (1I7Q) and *S. solfataricus* (1QDL). The alignment was generated by CE (37) and was printed using ESPript ([http://www-pgm1.ipbs.fr:8080/cgi-bin/nph-ESPript\\_exe.cgi](http://www-pgm1.ipbs.fr:8080/cgi-bin/nph-ESPript_exe.cgi)). The secondary structural elements of PabB are shown in black above the alignment ( $\beta$  for sheet,  $\alpha$  for helix, and TT for turn) and were assigned by DSSP (39). The numbering of PabB and the TrpE sequences from *Se. marcescens* and *S. solfataricus* are given at the left of each line. Conserved residues are shaded blue. Residues buried in the TrpE–TrpE interface of the *Se. marcescens* heterotetramer are shaded red, and those at the TrpE–TrpG interface are shaded green; R367 and R379 of *Se. marcescens* TrpE (equivalent to R311 and V323 of *E. coli* PabB and R272 and V284 of *S. solfataricus* TrpE) make contact with both the second TrpE subunit and a TrpG chain and are shaded pink. Residues underlined with a red bar comprise the tryptophan-binding pocket of PabB, and red triangles denote putative active site residues.

1.6 Å of C2 of the benzoate ring when the TrpE and PabB structures are superimposed.

*The Structure of PabB Reveals a Binding Site for Tryptophan.* An unanticipated finding from the structure elucidation of PabB was the presence of a tryptophan molecule buried in the sandwich formed by the  $\beta$ -sheets. The ligand is wedged into place by many interactions, which are shown in Figure 6. Interestingly, most of the polar contacts with the amino acid portion of the ligand arise from main chain carbonyl and amide atoms with the exception of the side chain of D404 that appears to interact with the tryptophan

carboxylate through a water molecule that is also hydrogen bonded to the hydroxyl group of Y396. The indole moiety of tryptophan is lodged in a hydrophobic pocket made up of the side chains of L34, F241, and I394. It is intriguing that the binding site is made up of a number of residues that are conserved among chorismate-utilizing enzymes, especially the anthranilate synthases, which are regulated by feedback inhibition.

The tryptophan is bound apparently quite strongly to the native enzyme, and is resistant to extensive dialysis or dilution. Indeed, noncovalently bound tryptophan can be



Scheme 2: Sequence Similarity among the Observed Tryptophan Binding Residues of *E. coli* PabB with Corresponding Residues in TrpE from the Anthranilate Synthases of *Se. marcescens*, *Sa. typhimurium*, and *S. solfataricus*, as Well as the Potential Tryptophan Binding Residues from *P. aeruginosa* PhnA, *Haemophilus influenzae* PabB, and *E. coli* EntC and MenF<sup>a</sup>

<i>E. coli</i> PabB	35	<b>LHS</b>	(6)	<b>YSRFDI</b>	(194)	<b>PFA</b>	(150)	IGY	(7)	DTS
<i>Haem</i> PabB	41	<b>ENS</b>	(5)	<b>-YF</b> FDI	(69)	<b>PKL</b>	(156)	FGI	(6)	QSA
Salty TrpE	38	<b>LES</b>	(6)	<b>DDLKSL</b>	(238)	<b>EMF</b>	(158)	VGY	(7)	DTC
Semar TrpE	37	<b>LES</b>	(6)	<b>ONLQSL</b>	(239)	<b>PMF</b>	(158)	VGY	(7)	DTC
Sulso TrpE	30	<b>LES</b>	(6)	<b>KARYSV</b>	(163)	<b>PMF</b>	(150)	VGF	(7)	EFA
<i>Paeru</i> PhnA	42	<b>FDC</b>	(6)	<b>AARRSV</b>	(238)	<b>PMF</b>	(158)	IGI	(7)	DTS
<i>E. coli</i> EntC	38	<b>FAR</b>	(6)	<b>NGDSPD</b>	(127)	<b>PMF</b>	(149)	VGW	(7)	EWV
<i>E. coli</i> MenF	39	<b>FDA</b>	(6)	<b>QOYTPQ</b>	(168)	<b>YHF</b>	(146)	AGY	(6)	EFC

<sup>a</sup> Residues highlighted in blue contribute main chain hydrogen bonds to tryptophan, whereas those shaded red indicate a hydrogen bonding interaction between the side chain and the ligand. Other residues either make hydrophobic contacts with the tryptophan or are structural elements of the binding pocket. Residues indicated in bold type are relatively conserved.

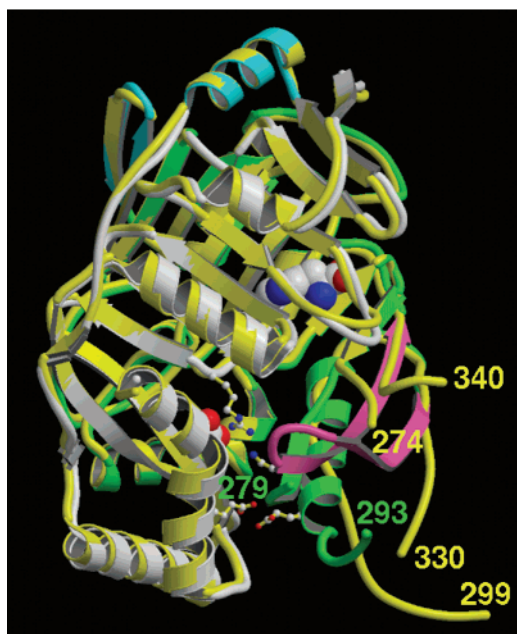


FIGURE 4: Structural attributes and differences of PabB from crystals grown in phosphate and in formate. (A) A view of the phosphate crystal lattice is presented showing the large solvent channels. The two yellow molecules in the center represent the asymmetric unit. The symmetry neighbors are shown in various shades of red and pink. (B) Structural superposition of the PabB monomer as seen in crystals grown in phosphate (yellow) and in formate (color scheme as described in the legend of Figure 1). Two significant differences in PabB can be seen when comparing the formate and phosphate structures. The unstructured region from residue 331 to 339 in the phosphate crystals, as well as in the unliganded monomer in the formate-grown crystals (not shown), becomes ordered in the formate-bound monomer, forming a two-stranded flap (pink) that appears to cover a portion of the active site. Additionally, residues 299–315 are in an extended conformation in phosphate crystals, but adopt a helical conformation (residues 301–315, green) in formate-grown crystals. Several active site residues are derived from this structured region. Shown are E302 (at the bottom of the helix) and K274 (in the adjacent green strand); also shown are E439 (bottom) and R410 (top) on the left side of the active site cleft. Formate is shown in space filling CPK colors adjacent to R410, and for orientation purposes, tryptophan is shown above the active site in space filling CPK colors. Yellow and green numbering refers to the ends of the crystallographically ordered segments in the phosphate and formate crystal forms, respectively.

identified in purified preparations of PabB even after dialysis against buffer for several days. In addition, the activity of the enzyme at a high (nanomolar) dilution is independent of the addition of exogenous tryptophan. The only approaches that so far have enabled the resolution of tryptophan from the enzyme require denaturation of PabB, and refolding studies have not yet been successful.

## DISCUSSION

It has been known for several years that the chorismate-utilizing enzymes involved in the biosynthesis of anthranilate, PABA, and isochorismate share significant sequence and mechanistic similarities (8, 9, 12–16, 20), and recent structural work has established the similar architectures for type I and type II anthranilate synthases (21–23), tetrameric enzymes with 2:2 TrpG:TrpE subunit stoichiometries. The overall fold of PabB described here corroborates the high level of structural similarity among this family of enzymes. In fact, at first glance, there appear to be more similarities than might be expected for enzymes with such distinct quaternary structures, catalytic functions, and regulatory attributes. The structure of PabB enables a consideration of these issues, as well as several hypotheses advanced from biochemical studies in solution. However, the structure also raises some provocative questions regarding the unique properties of ADC synthase, and general structure–function relationships for this entire enzyme family.

An intriguing difference among the chorismate-utilizing enzymes is the group of various quaternary structures that are seen for ADC synthase and the anthranilate synthases from *Sa. typhimurium*, *Se. marcescens*, and *S. solfataricus*. PabB is a monomer, at least in the absence of PabA, showing no tendency to self-associate as judged by analytical ultracentrifugation. Although it is clear that PabA and PabB must associate, at least transiently, for the efficient production of ADC from glutamine and chorismate (1, 6, 10), the interaction of PabB with PabA is not well-understood in molecular terms. Both proteins are reasonably stable in the absence of the other, and PabB itself, in the absence of PabA, can catalyze the formation of ADC in the presence of exogenous ammonia. By contrast, TrpE and TrpG can associate in apparently several different quaternary structures. Tetrameric structures of AS-st and AS-sm associate as TrpG–TrpE

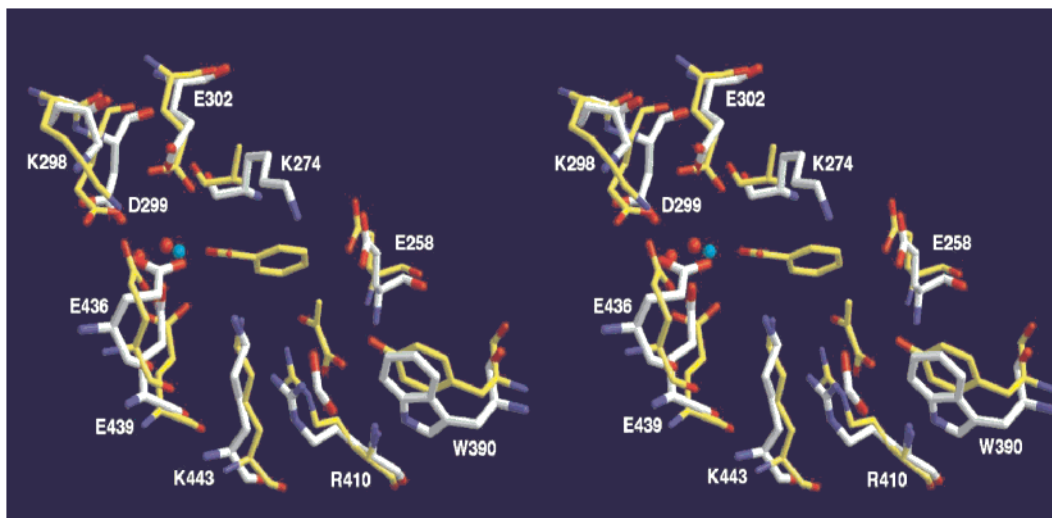


FIGURE 5: Active site environments of TrpE from *Se. marcescens* and that proposed for *E. coli* PabB. Stereoview of the side chain residues of AS-sm, shown in yellow, superimposed (37) onto PabB, which is represented in white. Benzoic acid and pyruvate from the 1I7Q coordinate set for AS-sm (23) are shown in yellow, whereas the formate seen in the one active site of PabB, close to the pyruvate site, is shown in white. The blue sphere represents a magnesium ion seen in AS-sm that is essential for catalysis, and the red spheres are water molecules that bridge the magnesium ion with E358 and E495 in the active site of TrpE.

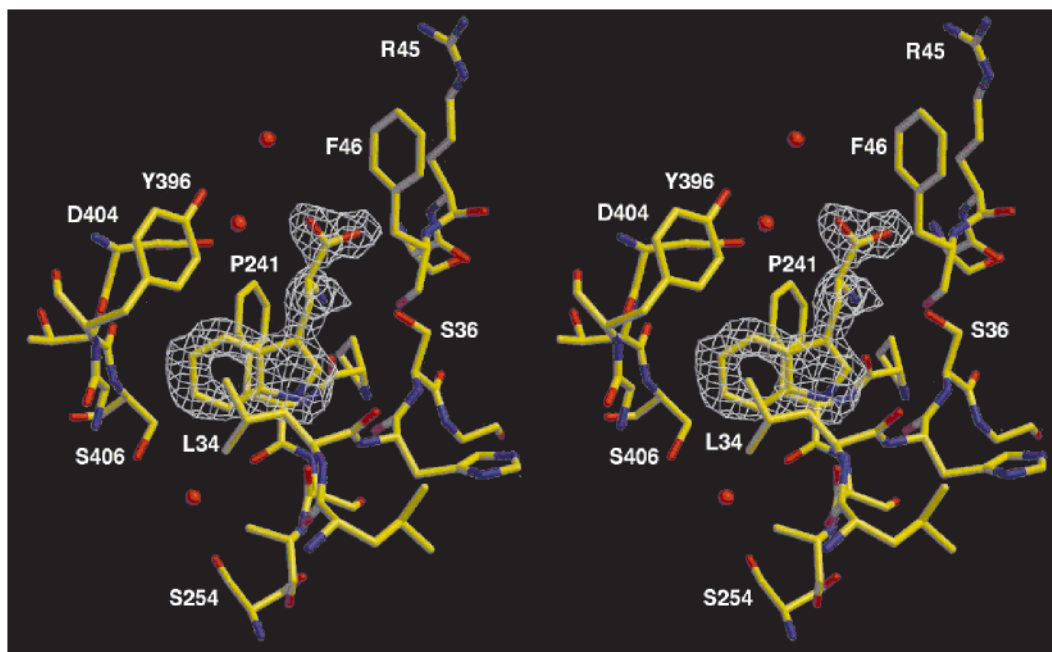


FIGURE 6: Stereoview of the tryptophan-binding site in *E. coli* PabB. The bound tryptophan is shown with its  $2F_o - F_c$  electron density plotted at  $1.5\sigma$ . Residues that comprise the binding site for tryptophan are indicated (see the text for details).

dimers primarily through TrpE subunits, whereas the TrpG–TrpE dimers of AS-ss associate through the TrpG subunit. However, the TrpE–TrpG interface throughout these various quaternary structures is remarkably similar. This unusual pattern of assembly may be related to tryptophan-promoted cooperativity in chorismate binding by AS-st and AS-sm (22, 42), and to the fact that tryptophan inhibition of AS-ss is not cooperative (21, 22, 43).

As can be seen in Figure 7, the interface of AS-sm that interacts with TrpG, and by analogy the interface of PabB that presumably interacts with PabA, comprise a limited surface that leads to the chorismate-binding site. An analysis of the surface area of these regions indicates that the TrpE–TrpG interface of AS-sm buries  $\sim 1487 \text{ \AA}^2$ , whereas the homologous surface on PabB for interaction with PabA is

only  $1067 \text{ \AA}^2$ . A similar analysis with AS-ss indicates that only  $1254 \text{ \AA}^2$  is buried at the TrpE–TrpG interface. Because the surface area estimated for the TrpE–TrpG interface of AS-ss is only  $\sim 15\%$  greater than that predicted for the PabB–PabA interaction and given the sharp contrast in quaternary structures seen for the two enzymes, there may also be significant differences between residues contributed from the TrpG subunit in AS and those from PabA in ADC synthase. Accordingly, although there are several residues among the enzymes that are highly conserved at this interface, there are also some significant differences. A 16-amino acid gap can be seen in PabB that corresponds to residues 106–121, including and surrounding helix  $\alpha 3$  in AS-sm (and AS-st), and which contribute potentially important interactions with the *Serratia* and *Salmonella* glutam-

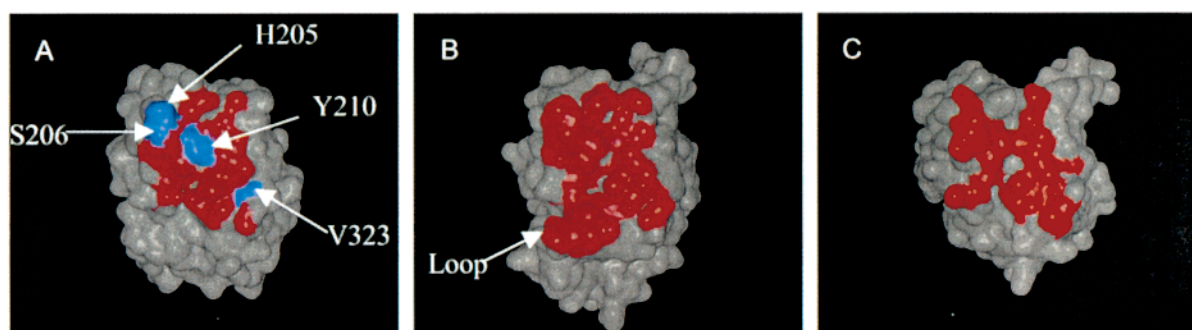


FIGURE 7: Space filling models of the surfaces of PabB and TrpE from the anthranilate synthases of *Se. marcescens* and *S. solfataricus* that interact with companion amidotransferase subunits: (A) *E. coli* PabB, (B) *Se. marcescens* TrpE, and (C) *S. solfataricus* TrpE. Colored regions of panel A show the surface of PabB that is buried by TrpG when superimposed on the TrpE–TrpG complex of *Se. marcescens*. The red regions of panels B and C show the TrpE surface of the *Se. marcescens* and *S. solfataricus* enzymes, respectively, buried by TrpG. Side chains colored red indicate amino acids that are conserved among the three interfaces, and those colored blue represent nonconserved residues. Amino acid residues in *E. coli* PabB that differ from corresponding residues in the TrpE subunits of anthranilate synthases from *Se. marcescens* and *S. solfataricus* are indicated in panel A and noted by arrows. The loop indicated in panel B is not present in either of the other proteins.

inase subunit (Figure 7B). There are also a number of single amino acid changes between PabB and the TrpE subunits at the interface. The surfaces shaded blue on PabB in Figure 7 correspond to residues H205, S206, Y210, and V323, which are not conserved in the TrpE sequences of oligomeric AS variants. Thus, the limited surface area for interaction on PabB, and the variation of several key residues and structural elements at this interface, suggest why its association with PabA is not as tight as that seen for TrpE and TrpG in anthranilate synthases, and may explain the inability to isolate intact ADC synthase complexes with the same level of ease as seen for anthranilate synthases.

Attempts were made to undertake a similar analysis of the region of PabB analogous to the TrpE–TrpE interface of AS-st and AS-sm to shed light on why PabB is monomeric whereas the TrpE subunits in these AS isozymes are dimeric. However, this effort was complicated by the fact that significant disorder is seen in both the formate- and phosphate-grown crystals of PabB for the residues in this region. Nonetheless, the structure-based sequence alignment shown in Figure 3 illustrates that a deletion in PabB after residue 279, corresponding to residues 333–339 of AS-sm, may be critical for dimerization. These residues immediately precede a region that comprises one side of the TrpE–TrpE interface in AS-sm (residues 342–353). In addition, residues 382–391 in AS-sm, which form the apposing side of the TrpE–TrpE interface, are not well-conserved in PabB (residues 323–332). These differences may account for the inability of PabB to dimerize, even at high protein concentrations.

Although the structure of PabB provides an important glimpse of the residues that may be important for substrate binding and catalysis, there are several outstanding questions that cannot be fully resolved by inspection of the unliganded and the formate-liganded enzyme. Indeed, despite the availability of four related structures, the mechanisms of ADC, anthranilate, and ADIC formation remain unclear. On one hand, the high level of conservation among active site residues suggests that proper orientation and complementarity of substrate binding may be a common feature of chorismate-utilizing enzymes. On the other hand, there are relatively few differences among the residues in the active sites of these

enzymes to explain the specificity for 2-amination and pyruvate elimination for anthranilate synthases, 2-hydroxylation for isochorismatase, and 4-amination for ADC synthase, which renders detailed predictions about mechanisms of PabB catalysis hazardous.

One possible clue as to the need for the third enzyme (ADC lyase) in PABA biosynthesis relative to the synthesis of anthranilate from chorismate and ammonia involves the position of K274 in the structure of ADC synthase. Lysine is found almost exclusively in this position in ADC synthases, whereas alanine is seen predominantly in anthranilate synthases. Although some exceptions to this distinction suggest that K274 may not have an essential role in the specificity of the reaction, the residue appears to partially occlude a region of the enzyme that may provide a “tunnel” between the active site of PabA where ammonia is generated and the active site of PabB. (Once a complex between PabA and PabB forms, there must presumably be a tunnel for the transfer of ammonia to act as a nucleophile to the activated cyclohexadiene ring of chorismate.) Specifically, the  $\epsilon$ -amino group of K274 appears to reside in the proximity of C2 of the benzoate ring when the TrpE and PabB structures are superimposed (Figure 5). Thus, the location and size of K274 may prevent the attack of ammonia on the C6 position of the cyclohexadiene ring of chorismate, preventing the formation of a putative 6-amino-6-dexoyisochorismate intermediate in anthranilate formation, and possibly favoring the formation of 4-amino-4-deoxychorismate, the substrate for ADC lyase. It is also possible that previous proposals for the enzymic synthesis of ADC that involve the pyruvoyl side chain and a bicyclic intermediate (9) may merit further consideration in light of the new structural information.

The striking discovery of tryptophan embedded firmly in the structure of PabB points clearly to its evolutionary relationship to the TrpE subunits of anthranilate synthase, and raises immediate questions about its function. The presence of tryptophan in all the PabB structures that have been determined, including the “closed” form of the enzyme with formate bound to the active site, is at first glance at odds with numerous biochemical and genetic results in which an effect of feedback modifiers on ADC synthase activity or the biosynthesis of PABA has not been detected. However,

the strong binding of tryptophan to PabB, as evidenced by its copurification, and the inability to resolve it by any means other than protein denaturation, suggests it is perhaps an integral component of the enzyme's structure.

On the basis of the sequences from several organisms for the genes of the tryptophan pathway and their homologues, Crawford suggested that *pabB* arose via gene duplication of *trpE* followed by divergence in which PabB descended from the original TrpE ancestor (44, 45). Thus, it is possible that the ancestral TrpE enzyme contained a structural tryptophan, and that its role in feedback inhibition of anthranilate biosynthesis was acquired later, and to varying extents, in its duplicated descendants. On the other hand, it is also possible that the activity of the TrpE ancestor was regulated by tryptophan and that while PabB retained, and possibly increased its affinity for the ligand, its allosteric effect was lost along with the capacity to form quaternary structure. In either event, the finding of tryptophan in the structure of PabB is consistent with Crawford's proposal of paralogous and orthologous events in its evolution. Interestingly, the residues that make up the tryptophan binding site are highly conserved not only between PabB and the feedback-regulated anthranilate synthases but also in the EntC and MenF isochorismate synthases of *E. coli*, and PhnA,<sup>2</sup> the anthranilate synthase involved in phycocyanin biosynthesis in *Pseudomonas aeruginosa*. This raises the interesting possibility that tryptophan may play a structural role in the folds of these proteins as well.

The crystal structure for PabB provides a rationale for the effects of amino acid substitutions on its association with PabA and ADC synthase activity. Nichols has characterized several classes of *pabB* mutants in terms of the inability of altered chains to form a complex with PabA, to utilize glutamine as a source of ammonia, and to catalyze the production of ADC using ammonia (11). Some of the catalytically defective mutants, in particular, T270G, R271G, G275I, and H339I, are in the proximity of the active site, and disruption of local stereochemistry may lead to losses in catalysis. Some of the substitutions in PabB that are unable to associate with PabA, including R316H, P371L, R311K, and E202G, are located on the surface of the enzyme that is homologous to the interface of the TrpE-TrpG interaction in AS. Recent data from our laboratory indicate that PabB possesses a micromolar affinity for the substrate chorismate, and that PabA and PabB associate more strongly than previously estimated, even in the absence of ligands (47). It will be of interest, therefore, to examine the stereochemical details of the interactions of these and other residues in structures of PabB in complex with chorismate and with PabA to shed more light on the common and unique features of this interesting reaction mechanism.

## ACKNOWLEDGMENT

We are indebted to Gary Gilliland for his interest and support of this work and are grateful to Kathryn E. Fisher

for the initial cloning of PabB and to Martin Mayhew, Marsha Holden, Vincent Vilker, and other members of the Bioprocess Engineering Group at the National Institute of Standards and Technology for plasmid DNA, highly purified chorismate, and advice. Certain commercial materials, instruments, and equipment are identified in this paper to specify the experimental procedure as completely as possible. In no case does such identification imply a recommendation or endorsement by the National Institute of Standards and Technology, nor does it imply that the materials, instruments, or equipment identified is necessarily the best available for the purpose.

## REFERENCES

- Nichols, B. P., Seibold, A. M., and Doktor, S. Z. (1989) *J. Biol. Chem.* 264, 8597–8560.
- Walsh, C. T., Erion, M. D., Walts, A. E., Delany, J. J., and Berchtold, G. A. (1987) *Biochemistry* 26, 4734–4745.
- Ye, Q. Z., Liu, J., and Walsh, C. T. (1990) *Proc. Natl. Acad. Sci. U.S.A.* 87, 9391–9395.
- Anderson, K. S., Kati, W. M., Ye, Q.-Z., Liu, J., Walsh, C. T., Benesi, A. J., and Johnson, K. A. (1991) *J. Am. Chem. Soc.* 113, 3198–3200.
- Viswanathan, V. K., Green, J. M., and Nichols, B. P. (1995) *J. Bacteriol.* 177, 5918–5923.
- Green, J. M., and Nichols, B. P. (1991) *J. Biol. Chem.* 266, 12971–12975.
- Green, J. M., Merkel, W. K., and Nichols, B. P. (1992) *J. Bacteriol.* 174, 5317–5323.
- Zalkin, H., and Smith, J. L. (1998) *Adv. Enzymol.* 72, 87–144.
- Walsh, C. T., Liu, J., Rusnak, F., and Sakaitani, M. (1990) *Chem. Rev.* 90, 1105–1130.
- Roux, B., and Walsh, C. T. (1992) *Biochemistry* 31, 6904–6910.
- Rayl, E. A., Green, J. M., and Nichols, B. P. (1996) *Biochim. Biophys. Acta* 1996, 81–88.
- Goncharoff, P., and Nichols, B. P. (1988) *Mol. Biol. Evol.* 5, 531–548.
- Kozlowski, M. C., Tom, N. J., Seto, C. T., Sefler, A. M., and Bartlett, P. A. (1995) *J. Am. Chem. Soc.* 117, 2128–2140.
- Kaplan, J. B., and Nichols, B. P. (1983) *J. Mol. Biol.* 168, 451–468.
- Goncharoff, P., and Nichols, B. P. (1984) *J. Bacteriol.* 159, 57–62.
- Kaplan, J. B., Merkel, W. K., and Nichols, B. P. (1985) *J. Mol. Biol.* 183, 327–340.
- Zalkin, H. (1985) *Methods Enzymol.* 113, 287–292.
- Ito, J., and Yanofsky, C. (1966) *J. Biol. Chem.* 241, 4112–4114.
- Zalkin, H., and Hwang, L. H. (1971) *J. Biol. Chem.* 246, 6899–6907.
- Rauschel, F. M., Thoden, J. B., and Holden, H. M. (1999) *Biochemistry* 38, 7891–7899.
- Knöchel, T., Ivens, A., Hester, G., Gonzalez, A., Bauerle, R., Wilmanns, M., Kirschner, K., and Jansonius, J. N. (1999) *Proc. Natl. Acad. Sci. U.S.A.* 96, 9479–9484.
- Morollo, A. A., and Eck, M. J. (2001) *Nat. Struct. Biol.* 8, 243–247.
- Spraggon, G., Kim, C., Nguyen-Huu, X., Yee, M. C., Yanofsky, C., and Mills, S. E. (2001) *Proc. Natl. Acad. Sci. U.S.A.* 98, 6021–6026.
- Doublet, S. (1997) *Methods Enzymol.* 276, 523–530.
- Rubinson, K. A., Ladner, J. E., Tordova, M., and Gilliland, G. L. (2000) *Acta Crystallogr. D* 56, 996–1001.
- Howard, A. (2000) in *7th IUCR Symposium on Crystallographic Computing* (Bourne, P. E., and Watenpaugh, K., Eds.) International Union of Crystallography, Oxford.
- Pflugrath, J. W. (1999) *Acta Crystallogr. D* 55, 1718–1725.

<sup>2</sup> The recent explosion of DNA sequence information has resulted in at least two functionally unrelated proteins being annotated as PhnA. Here, PhnA refers specifically to the second anthranilate synthase from *P. aeruginosa* identified by Crawford (46), which corresponds to protein identified as PA1001 in the TIGR comprehensive microbial resource database (<http://www.tigr.org/CMR>).

28. Usón, I., and Sheldrick, G. M. (1999) *Curr. Opin. Struct. Biol.* 9, 643–648.
29. La Fortelle, E. d., and Bricogne, G. (1997) *Methods Enzymol.* 276, 472–494.
30. Abrahams, J. P., and Leslie, A. G. W. (1996) *Acta Crystallogr. D52*, 30–42.
31. Perrakis, A., Morris, R. J., and Lamzin, V. S. (1999) *Nat. Struct. Biol.* 6, 458–463.
32. Brünger, A. T., Adams, P. D., Clore, G. M., DeLano, W. L., Gros, P., Grosse-Kunstleve, R. W., Jiang, J.-S., Kuszewski, J., Nilges, M., Pannu, N. S., Read, R. J., Rice, L. M., Simonson, T., and Warren, G. L. (1998) *Acta Crystallogr. D54*, 905–921.
33. McRee, D. E. (1999) *Practical Protein Crystallography*, 2nd ed., Academic Press, San Diego.
34. Sheldrick, G. M., and Schneider, T. R. (1997) *Methods Enzymol.* 277, 319–343.
35. Roussel, A., Inisan, A.-G., and Cambillau, C. (1996) Turbo-Frodo, AFMB and Bio Graphics, Marseille, France.
36. Berman, H. M., Westbrook, J., Feng, Z., Gilliland, G., Bhat, T. N., Weissig, H., Shindyalov, I. N., and Bourne, P. E. (2000) *Nucleic Acids Res.* 28, 235–242.
37. Shindyalov, I. N., and Bourne, P. E. (1998) *Protein Eng.* 11, 739–747.
38. Laskowski, R. A., MacArthur, M. W., Moss, D. S., and Thornton, J. M. (1993) *J. Appl. Crystallogr.* 26, 283–291.
39. Kabsch, W., and Sander, C. (1983) *Biopolymers* 22, 2577–2637.
40. Hutchinson, E. G., and Thornton, J. M. (1996) *Protein Sci.* 5, 212–220.
41. Collaborative Computational Project No. 4 (1994) *Acta Crystallogr. D50*, 760–763.
42. Caligiuri, M. G., and Bauerle, R. (1991) *J. Biol. Chem.* 266, 8328–8335.
43. Tutino, M. L., Tosco, A., Marino, G., and Sannia, G. (1997) *Biochem. Biophys. Res. Commun.* 230, 306–310.
44. Crawford, I. P. (1989) *Annu. Rev. Microbiol.* 43, 567–600.
45. Crawford, I. P., and Milkman, R. (1991) in *Evolution at the Molecular Level* (Selander, R. K., Clark, A. G., and Whittam, T. S., Eds.) pp 77–95, Sinauer Associates, Inc., Sunderland, MA.
46. Essar, D. W., Eberly, L., Hadero, A., and Crawford, I. P. (1990) *J. Bacteriol.* 172, 884–900.
47. Parsons, J. F., Jensen, P. Y., Pachikara, A. S., Eisenstein, E., and Ladner, J. E. (2001) *FASEB J.* 15 (4), 9190.

BI015791B